Journal of Solid State Chemistry 184 (2011) 764–769

Contents lists available at ScienceDirect

Journal of Solid State Chemistry

journal homepage: www.elsevier.com/locate/jssc

Hierarchical Ag/ZnO micro/nanostructure: Green synthesis and enhanced photocatalytic performance

Shuyan Gao*, Xiaoxia Jia, Shuxia Yang, Zhengdao Li, Kai Jiang*

College of Chemistry and Environmental Science, Henan Normal University, 46 Jianshe Street, Xinxiang 453007, Henan, PR China

ARTICLE INFO

Article history:
Received 27 October 2010
Received in revised form
21 December 2010
Accepted 17 January 2011
Available online 1 February 2011

Keywords:
Hydrothermal synthesis
Hierarchical Ag/ZnO micro/nanostructure
Photodegradation
Green chemistry

ABSTRACT

Ag/ZnO metal–semiconductor nanocomposites with hierarchical micro/nanostructure have been prepared by the hydrothermal synthesis in the presence of bovine serum albumin (BSA). The results suggest that this biomolecule-assisted hydrothermal method is an efficient route for the fabrication of Ag/ZnO nanocomposites by using BSA both a shape controller and a reducing agent of Ag^+ ions. Moreover, Ag nanoparticles on the ZnO act as electron sinks, improving the separation of photogenerated electrons and holes, increasing the surface hydroxyl contents of ZnO, facilitating trapping the photoinduced electrons and holes to form more active hydroxyl radicals, and thus, enhancing the photocatalytic efficiency of ZnO. This is a good example for the organic combination of green chemistry and functional materials.

1. Introduction

ZnO is an ideal photocatalyst because it has similar band gap energy to that of TiO_2, and thus the similar phototocatalytic mechanism and capacity. However, some studies have confirmed that ZnO, especially on the nanometer-scale, exhibits better efficiency than TiO_2 in photocatalytic degradation of some dyes, even in aqueous solution in some cases [1–4]. Parellelly, the modification of semiconductors with noble metals has attracted significant attention especially in heterogeneous photocatalysis. Nowadays, it is believed that surface states can be greatly improved by catalytic noble metals [5–7], such as Ag. It is found that Ag nanoparticles and oxygen vacancy defects on the surface of ZnO nanocrystals can trap the photogenerated electrons from the semiconductor, benefit the separation of photogenerated electron–hole pairs, allow the holes to form hydroxyl radicals, thus enhancing the photocatalytic activity [8].

However, nanometer-scaled materials, such as nanoparticles and nanorods, with a high surface-to-volume ratio tend to aggregate during the preparation and photocatalysis process, which results in the reduction of the photocatalytic efficiency. An available way to prevent the nanoparticles from aggregation and maintain the high photocatalytic efficiency is to organize these nanoscale materials into hierarchical structures [9]. In general, the preparation of hierarchical metal–semiconductor nanocomposites has two steps [10,11]. First, the semiconductor material was prepared into sol solution, and added metal salts. Then metal salts in the semiconductor sol solution was irradiated or reduced by UV light. However, this method was complicated, and most importantly, the reduction process often leaded metal to self-nucleation and produced the unexpected isolated metal nanoparticles. In order to overcome this shortcoming, we focus on one-step green method to prepare hierarchical Ag/ZnO nanocomposites. Recently, we succeeded in synthesizing hierarchical Ag/ZnO micro/nanostructure by the hydrothermal synthesis of $Zn(AC)_2$ in the presence of bovine serum albumin (BSA). This hierarchical micro/nanostructure is assembled by nanorods. Compared with a large number of reports on the synthesis of Ag/ZnO heterostructures, this method simplifies experimental procedure, shortens reaction time, reduces reaction temperature and is a green synthetic route. Moreover, Ag nanoparticles on the ZnO act as electron sinks, improving the separation of photogenerated electrons and holes, increasing the surface hydroxyl contents of ZnO, facilitating trapping the photoinduced electrons and holes to form more active hydroxyl radicals, and thus, enhancing the photocatalytic efficiency of ZnO.

2. Experimental section

2.1. Synthesis of Ag/ZnO nanocomposites

All the reagents, including zinc acetate ($Zn(AC)_2$ $2H_2O$), 28 wt% aqueous ammonium solution, silver nitrate ($AgNO_3$), BSA, and ethanol, were analytical grade and used without further purification.

* Corresponding authors. Fax: +86 373 3326544.
E-mail addresses: shuyangao@htu.cn (S. Gao), jk@htu.cn (K. Jiang).

0022-4596/$ - see front matter © 2011 Elsevier Inc. All rights reserved.
doi:10.1016/j.jssc.2011.01.025

The synthesis of Ag/ZnO nanocomposites is as follows. Zinc acetate (5.0×10^{-3} M, 30 mL) and BSA (1.8×10^{-5} M, 1.3 mL) and an appropriate amount of silver nitrate solution (2.8×10^{-2} M) were mixed with agitation in a beaker. Then, ethanol (8 mL) and an aqueous ammonia solution (1.1 mL, 28 wt%) were added dropwise to the above mixture. The resulting solution was transferred into a 50 mL Teflon-lined autoclave and heated at 373 K for 7 h. When the reactions were completed, the precipitates were collected, washed with deionized water and ethanol several times, and finally dried in air naturally.

2.2. Sample characterizations

The powder X-ray diffraction (XRD) patterns of the samples were recorded by a Bruker D8A X-ray diffractionmeter with Cu$K\alpha_1$ radiation ($\lambda=1.54056$ Å). Working voltage was 40 kV and current was 200 mA. The morphologies of the as-prepared samples were observed by field-emission scanning electron microscope (FESEM) in the XL 30 ESEM FEG scanning electron microscope, and the working voltage was 20 kV. Chemical compositions were analyzed with an X-ray energy dispersive spectroscope (EDS) attached to the SEM. Microstructure analysis was carried out by high resolution transmission electron microscopy (HRTEM), taken with a JEOL JEM-2010 transmission electron microscope. The elemental and chemical states of the as-prepared samples in this heterostructure were determined by X-ray photoelectron spectroscopy (XPS) in the ESCALab MKII X-ray photoelectron spectrometer with Mg$K\alpha$ radiation (1486.6 eV). As an internal reference for the absolute binding energies, the C 1*s* peak of hydrocarbon contamination was used. Using the atomic sensitivity factors, the actual content of Ag for each sample was calculated by the relation:

$$\mathrm{Ag\ (at\%)} = (I_{Ag}/\delta_{Ag})/(I_{Ag}/\delta_{Ag}+I_{Zn}/\delta_{Zn}+I_O/\delta_O)$$

where I_{Ag}, I_{Zn}, and I_O are the area under the deconvoluted XPS curves of Ag 3*d*, Zn $2p_{3/2}$, and O 1*s*, respectively; σ_{Ag}, σ_{Zn}, and σ_O are the corresponding atomic sensitivity factors for Ag 3*d* (5.198), Zn $2p_{3/2}$, (3.354), and O 1*s* (0.711), respectively [12].

2.3. Photocatalytic tests

The photocatalytic activity of the Ag/ZnO photocatalyst was evaluated by measuring the degradation rate of Orange G (OG) under ultraviolet (UV) light illumination. OG is a nonbiodegradable synthetic dye with a molecular formula of $C_{16}H_{10}N_2O_7S_2Na_2$, widely used in the textile industry. A cylindrical reactor surrounded by a circulating water jacket maintained at a constant temperature throughout the experiment was used and the UV light was provided by a 250 W high-pressure fluorescent Hg lamp (Institute of Electrical Light Source, Beijing; the strongest emission at 365 nm). A mixture of 50 mL of 10 ppm OG aqueous solution and 0.05 g of each photocatalyst was agitated in the dark for 20 min in a photoreactor to ensure establishment of adsorption equilibrium of the dye on the catalyst surface. Light intensity was measured using TU-1810 UV–vis spectrophotometer (Beijing Purkinje General Instrument Co., Ltd.).

3. Results and discussion

3.1. Reaction mechanism

At the initial stage of the reaction, Zn^{2+} and Ag^+ coordinate with BSA, respectively. With the dropwise addition of ammonia, $Zn(OH)_2$ and AgOH were slowly formed. When the amount of ammonia increases, $Zn(OH)_2$ and AgOH will be gradually dissolved into $Zn(NH_3)_4^{2+}$, $Zn(OH)_4^{2-}$, $Ag(NH_3)_2^+$, and $Ag(OH)_2^-$, respectively, as shown by the following equations:

$$NH_3+H_2O\rightarrow NH_4^+ +OH^- \quad (3.1)$$

$$Zn^{2+}+2OH^-\rightarrow Zn(OH)_2\downarrow \quad (3.2)$$

$$Ag^+ +OH^-\rightarrow AgOH\downarrow \quad (3.3)$$

$$Zn(OH)_2+2OH^-+4NH_3\rightarrow Zn(OH)_4^{2-}+4NH_3\rightarrow Zn(NH_3)_4^{2+}+4OH^- \quad (3.4)$$

$$AgOH+OH^-+2NH_3\rightarrow Ag(OH)_2^-+2NH_3\rightarrow Ag(NH_3)_2^+ +2OH^- \quad (3.5)$$

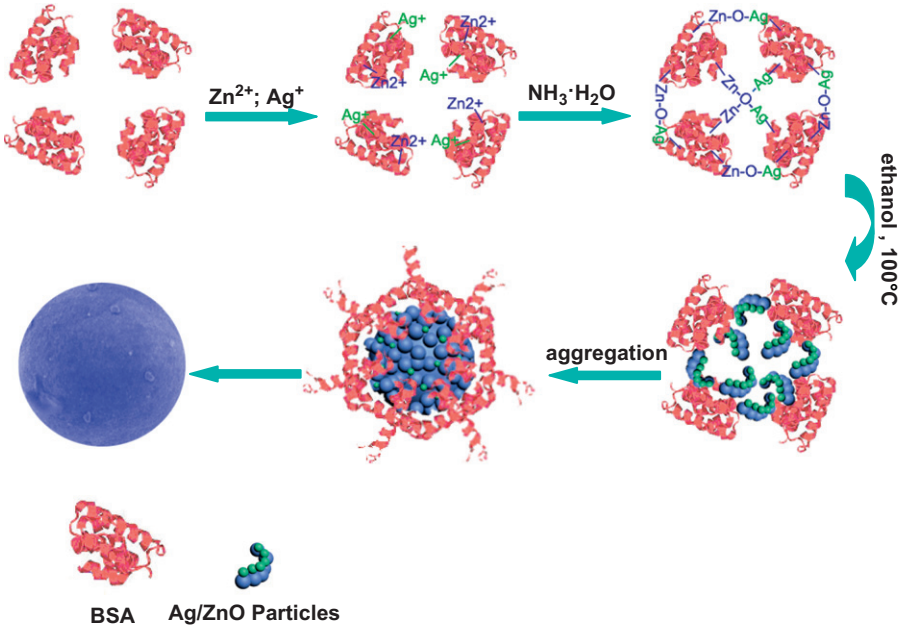

Fig. 1. Schematic graph of the growth mechanism of the hierarchical Ag/ZnO micro/nanostructure in the presence of BSA.

Under alkaline thermal condition, intermolecular dehydrolysis between $Zn(OH)_4^{2-}$ and $Ag(OH)_2^-$ may occur, leading to the formation of Ag_2O/ZnO nuclei through a Zn–O–Ag bond [13]. At the growth stage, a Zn–O–Ag bond can be formed between Ag and ZnO, leading to the formation of Ag/ZnO nanocomposites [13]. The schematic growth mechanism is shown in Fig. 1:

$$Zn(OH)_4^{2-} + 2Ag(OH)_2^- \xrightarrow{\text{co-dehydrolysis}} Ag_2O/ZnO \quad (3.6)$$

$$Ag_2O/ZnO + \text{ethanol} \rightarrow Ag/ZnO \quad (3.7)$$

It should be mentioned that, during the whole preparation process, due to the complexation of Ag^+ with ammonia in the solution, the standard redox potential of $Ag(NH_3)_2^+/Ag$(+0.38 eV) was much lower than that of Ag^+/Ag(+0.8 eV) [14], so the Ag_2O will be preferentially reduced by ethanol than $Ag(NH_3)_2^+$ will be, which leads to the formation of Ag nanoparticles on the ZnO surface.

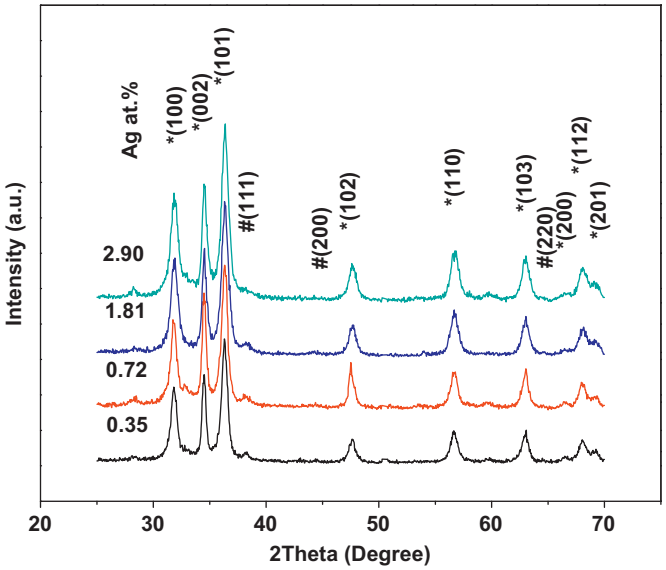

Fig. 2. XRD patterns of the Ag/ZnO samples with various silver contents.

3.2. Crystal structure and microstructure of the as-prepared Ag/ZnO samples

3.2.1. XRD analysis

The XRD patterns of the as-synthesized samples with different Ag contents are shown in Fig. 2. It is found that there are two sets of diffraction peaks for each sample, indicating that the as-synthesized samples are composite materials. Those marked with "#" can be indexed to hexagonal wurtzite ZnO (JCPDS file no. 36-1451), while the others marked with "*" can be indexed to face-centered-cubic (fcc) metallic Ag (JCPDS file no. 04-0783). Comparing with the diffraction peaks of pure ZnO, no characteristic peaks of impurities and other phases such as $Zn(OH)_2$ and Ag_2O are observed. In addition, negligible changes of all diffraction peak positions and lattice parameters of ZnO in all Ag/ZnO samples compared to that of pure ZnO suggest that Ag does not incorporate into the lattice of ZnO, but as metal deposit on the surface.

3.2.2. FESEM, EDS, and HRTEM analyses

The representative FESEM patterns of the samples are shown in Fig. 3. The low-magnified FESEM observation (Fig. 3a) shows that the morphology is hierarchically micro/nano-structured microspheres ranging from 2 to 5 μm in diameter. Closer observations (Figs. 3b and c) show that the surface of the product is smooth. The highly magnified FESEM image of a fragment of the broken sphere (Fig. 3d) reveals that the structure of these spheric architectures is built from a single layer of radially oriented nanorods, self-wrapping to form hollow interiors with 2–5 μm in outer diameter. It is worth noting that all the constituent nanorods are radially aligned with their growth axes perpendicular to the surface of the microspheres without any substrate support [15–17].

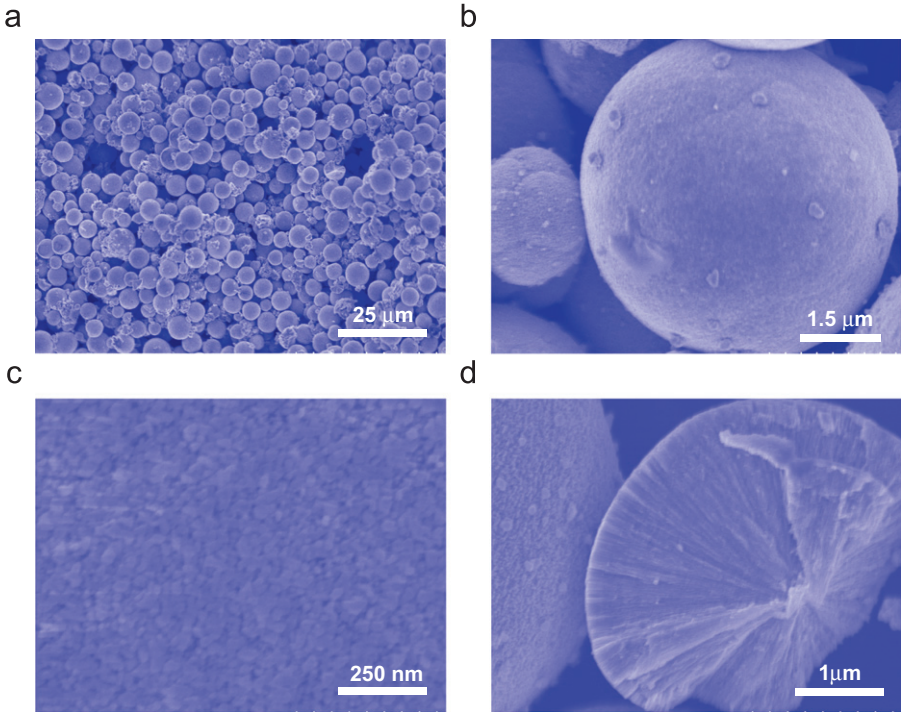

Fig. 3. Representative FESEM images of the as-synthesized Ag/ZnO samples: (a) a low magnified panoramic view, (b) an individual microsphere, (c) a high magnified FESEM image taken from the squared region, and (d) a fragment of one broken microsphere.

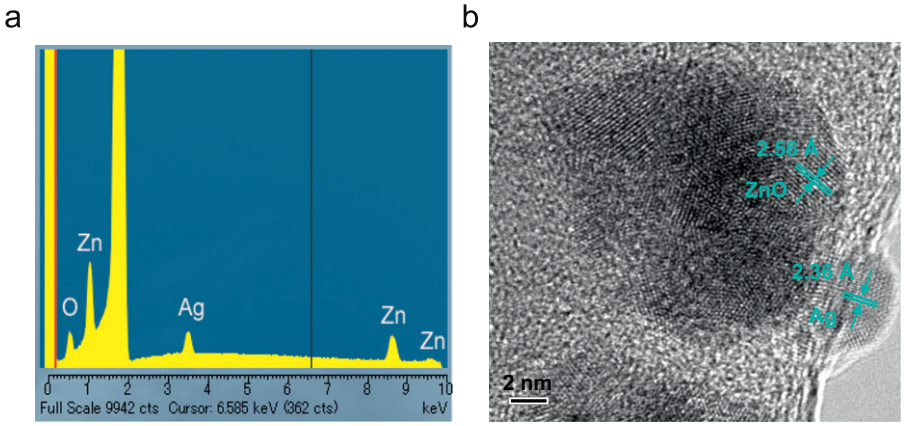

Fig. 4. (a) The elemental spectra of Ag/ZnO reveled by EDS analysis and (b) HRTEM image of the product.

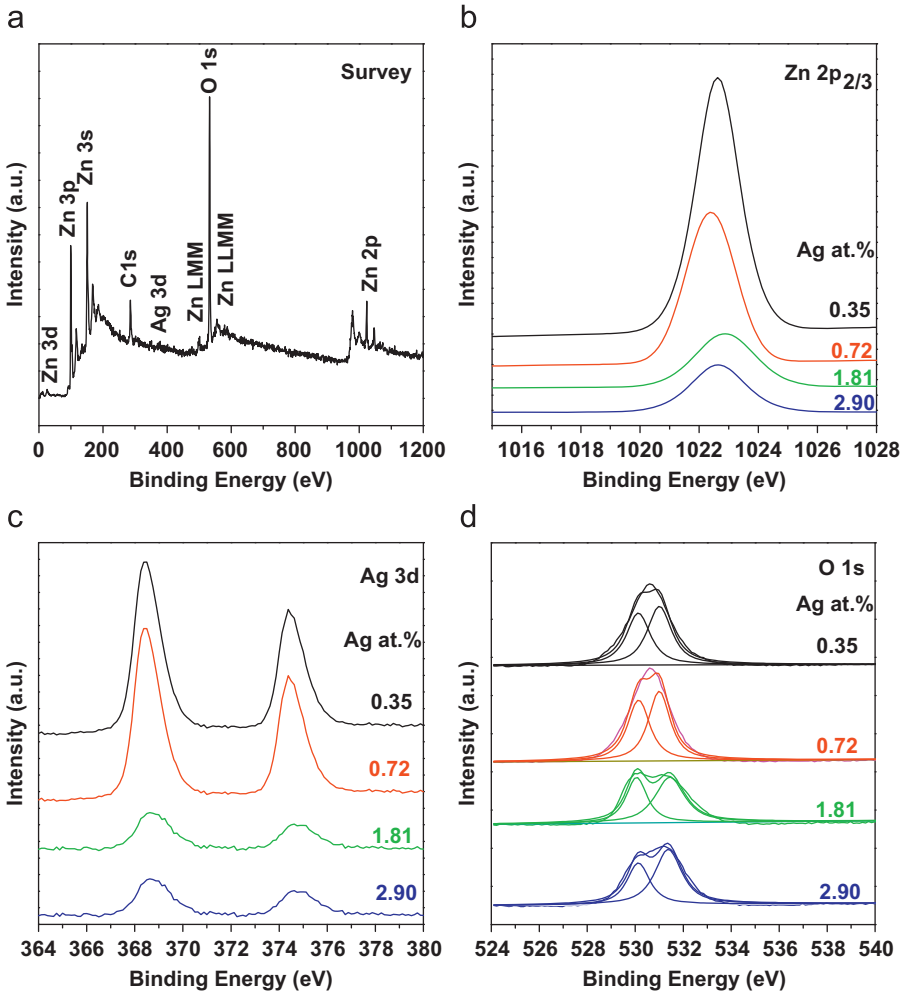

Fig. 5. (a) Representative XPS survey spectrum of Ag/ZnO sample with a Ag content of 1.81 at%. The XPS full spectra of (b) Zn $2p_{3/2}$, (c) Ag 3*d*, and (d) O 1*s* of the as-prepared Ag/ZnO samples with various Ag contents.

Fig. 4a gives the elemental spectra of the Ag/ZnO micro/nanostructure revealed by EDS analysis. It indicates that the Ag/ZnO hierarchical structure is only composed of three elements, Zn, Ag, and O. Fig. 4b gives the HRTEM image of the interface structures between Ag and ZnO crystals. The plane fringe with a 2.36 Å crystalline plane spacing is assigned to the Ag {111} planes. The spacing between adjacent lattice fringes is 2.56 Å, which is close to the *d* spacing of the (002) plane of ZnO. These indicate that Ag nanoparticles is on the ZnO surface, not incorporating into the lattice of ZnO.

3.2.3. *XPS analysis*

To clarify the elemental and chemical state of Ag in the sample, XPS spectra were carried out. Fig. 5a shows the scan survey spectra for the representative Ag/ZnO sample with Ag

content of 1.81 at%. All of the peaks on the curve can be ascribed to Ag, Zn, O, and C elements, while C 1*s* at 284.8 eV is due to the hydrocarbon from the XPS instrument itself [18]. The positions of Zn $2p_{3/2}$ peak for all Ag/ZnO samples (Fig. 5b) are nearly at the same value of 1021.4 eV, which confirms that Zn element exists mainly in the form of Zn^{2+} chemical state on the sample surfaces.

Fig. 5c provides the high-resolution XPS spectra of Ag in the samples. The Ag $3d_{5/2}$ peak appears at a binding energy of 367.4 eV. Here, interestingly, the $3d_{5/2}$ peak of Ag in our work was found to shift obviously to the lower binding energy compared with the standard value (about 368.2 eV for bulk Ag). This confirms the interaction between Ag and ZnO nanocrystals as the binding energy of monovalent Ag is known to be much lower than that of zerovalent Ag. Similar results were also found in previous work [5,8]. It is suggested that the shift of the binding energy of Ag $3d_{5/2}$ should be mainly ascribed to the interaction between the Ag nanoparticle and ZnO. When the Ag nanoparticle and ZnO attach together, they adjust the position of their corresponding Fermi energy levels to the same value (Fig. 7).

Fig. 5d shows the O 1*s* peaks for all of the samples under study. It can be seen that all of the O 1*s* peaks are somewhat asymmetric, suggesting that there are at least two kinds of oxygen species on the sample surface. In all XPS curves, the deconvoluted peak marked with "α" is closely associated with the lattice oxygen (O_L) of ZnO and its position is at about 530 eV, while the other peak marked with "β" is attributed to the oxygen of surface hydroxyl (OH) and its position is at about 531.5 eV [19–21]. Since the surface hydroxyl plays a crucial role in trapping photoinduced electrons and holes, it can be concluded that Ag deposition can modify the surface hydroxyl contents of hierarchically micro/nano-structured ZnO spheres.

3.3. Photocatalytic performance

The photocatalytic activities of the Ag/ZnO with various Ag contents are evaluated by measuring the degradation of OG in aqueous solution under UV light irradiation. The time-dependent absorbance spectra of the dye solution are shown in Fig. 6a in the presence of hierarchically micro/nano-structured ZnO spheres with Ag content of 1.81 at%. It is obvious that the absorbance peaks at 250, 331, and 472 nm are reduced significantly, indicating the degradation of the dye molecules. After the illumination time of 70 min, the initial OG solution can be totally decolorized.

The photocatalytic experimental data can be converted to a linear pattern using pseudo-first kinetics model, and the results are shown in Fig. 6b. Also, as photocatalytic reference, pure ZnO is used to evaluate the activity of Ag/ZnO samples. It can be seen from Fig. 6b that the photocatalytic performance can be significantly improved by depositing an appropriate amount of Ag nanoparticles. It has been reported that Ag clusters and/or nanoparticles on the surface of ZnO nanocrystals act as a sink for the electrons, promote interfacial charge-transfer kinetics between the metal and the semiconductor, improve the separation of photogenerated electron–hole pairs, and thus enhance the photocatalytic activity of Ag/ZnO photocatalysts. Therefore, the higher the dispersity of Ag clusters and/or nanoparticles on the surface of ZnO is, the higher the photocatalytic activity of Ag/ZnO photocatalyst should be. This can be understood based on the proposed charged separation of Ag/ZnO under UV irradiation shown in Fig. 7. Because the bottom energy level of the conduction band (CB) of ZnO is higher than the new equilibrium Fermi energy level (E_f) of Ag/ZnO, the photoexcited electrons on the CB under UV irradiations could transfer from ZnO to the Ag nanoparticles. It has been proposed that the charge separation is the outcome of a Schottky barrier formed at the metal–semiconductor interface [22,23]. The possible mechanistic pathway of Ag/ZnO for degradation of OG can be proposed as follows [8]:

$$ZnO + h\nu(UV) \rightarrow ZnO(e_{cb}^- + h_{vb}^+) \quad (3.8)$$

$$Ag \rightarrow Ag^+ + e^- \quad (3.9)$$

$$e^- + O_2(ads) \rightarrow {}^{\bullet}O_2^- \xrightarrow{H^+} {}^{\bullet}O_2H \xrightarrow{{}^{\bullet}O_2H} O_2 + H_2O_2 \xrightarrow{e^-} O_2 + {}^{\bullet}OH + OH^- \quad (3.10)$$

$$Ag^+ + e^- \rightarrow Ag \quad (3.11)$$

$$h_{vb}^+ + OH^- \rightarrow {}^{\bullet}OH \quad (3.12)$$

$${}^{\bullet}OH + OG \rightarrow \text{degradation products} \quad (3.13)$$

However, it is found from Fig. 6b that as the Ag content increases, the photocatalytic performance of the Ag/ZnO has not been enhanced monotonously. When the Ag content is relatively lower (<1.81 at%), the photocatalytic activity of the Ag/ZnO increases with the increase of Ag content (ZnO <0.35 at% Ag/ZnO <0.72 at% Ag/ZnO <1.81 at% Ag/ZnO). On the other hand, when the Ag content is relatively higher (>1.81 at%), the photocatalytic activity of the Ag/ZnO decreases with the increase of Ag content (1.81 at% Ag/ZnO >2.90 at% Ag/ZnO). Thus the optimal Ag content is approximately 1.81 at%. Several groups have suggested that, at higher metal content than the optimal one, the over accumulations of electron on metal deposits could attract the photogenerated holes to the metal sites. This may encourage

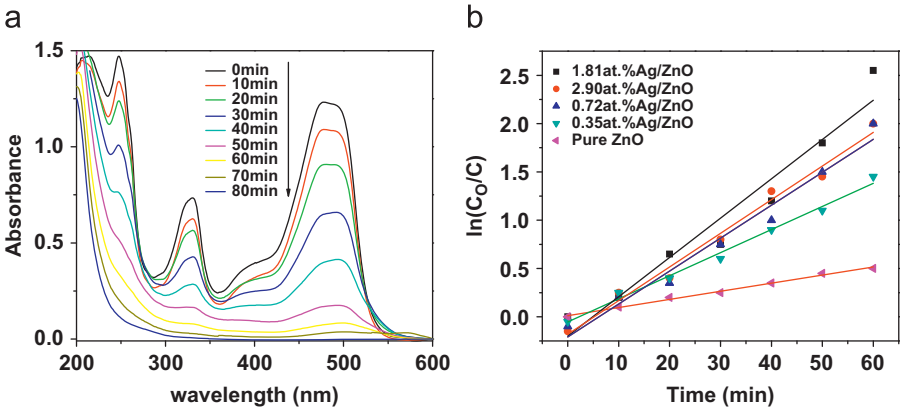

Fig. 6. (a) Time-dependent UV vis absorbance spectra of the OG solution in the presence of Ag/ZnO sample with Ag content of 1.81 at%. (b) The $\ln(C_0/C)$ versus time curves of photodegradation of OG. C_0 and C are the initial concentration after the adsorption equilibrium and the reaction concentration of OG, respectively. The experimental data are fitted using the pseudo-first-order kinetic equation: $\ln(C_0/C)=kt$.

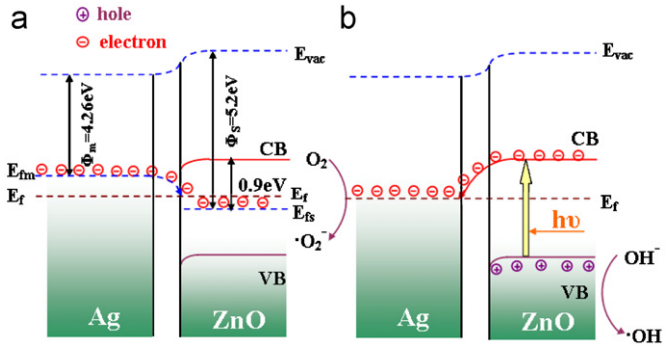

Fig. 7. (a) The band structures of Ag and ZnO junction and the Fermi energy level equilibrium without UV irradiation [8,29,30]. Because of the larger work function of ZnO, the Fermi energy level of ZnO (E_{fs}) is lower than that of Ag (E_{fm}), resulting in the transfer of electrons from Ag to ZnO until the two systems attain equilibrium and form the new Fermi energy (E_f). (b) The proposed charge separation process and the photocatalytic mechanism of as-prepared Ag/ZnO samples under UV irradiation. Due to that the energy level of CB for ZnO is higher than the Fermi energy level of Ag, the photoinduced electrons are transferred to the metallic Ag. Then the electrons in the Ag sinks can be trapped by the chemisorbed O_2 and the hole can be captured by the surface hydroxyl.

the recombination of charge carriers and the metal deposits reversely behave as recombinant centers [24,25]. In addition, higher surface loadings of metal deposits may decrease the catalytic efficiency of the semiconductor due to the reductive availability of semiconductor surface for light absorption and pollutant adsorption [26], and the resultant variation of the surface hydroxyl content of Ag/ZnO with different Ag content.

In the process of photocatalysis, after the photogenerated electrons and holes are separated from recombination, they can be trapped generally by the oxygen and surface hydroxyl, respectively, to produce ultimately the primary oxidizing species of the hydroxyl radicals (·OH), which plays a significant role in the photocatalytic oxidation process [13,27,28]. The more the surface hydroxyl content is, the more efficient the photocatalyst is [12]. From this point, we can reasonably conclude that the difference in photocatalytic activity is related to various contents of surface hydroxyl on the hierarchically micro/nano-structured ZnO spheres caused by different Ag contents. Therefore, the 1.81 at% Ag/ZnO sample, which has the highest surface hydroxyl content, exhibits the highest photocatalyst performance in our work.

4. Conclusion

In summary, Ag/ZnO metal–semiconductor nanocomposites have been synthesized through biomolecule-assisted hydrothermal method, which is a green synthetic route. The as-formed samples have uniform morphology, and show hierarchical micro/nanostructure. On the basis of the structural characterizations and photocatalytic results, the effect of Ag deposition on the structure and photocatalytic performance of ZnO can be summarized as follows: (i) Ag nanoparticles on the ZnO act as electron sinks, improving the separation of photogenerated electrons and holes; (ii) Appropriate contents of Ag deposition increase the surface hydroxyl contents of ZnO, facilitate trapping the photoinduced electrons and holes to form more active hydroxyl radicals, and thus, enhance the photocatalytic efficiency of ZnO. These results show that this green method can be an effectively extended to the development of photocatalysts with hierarchical structure, which are applicable in both environmental purification and energy production processes. It is a good example for the organic combination of green chemistry and functional materials.

Acknowledgments

The authors are grateful to the National Natural Science Foundation of China (no. 21071047), the Henan Provincial Natural Science Foundation of China (092300410196), and Natural Science Foundation of Educational Department of Henan Province (2008A150014).

References

[1] A.A. Khodja, T. Sehili, J.F. Pilichowski, P. Boule, J. Photochem. Photobiol. A 141 (2001) 231–239.
[2] N. Daneshvar, D. Salari, A.R. Khataee, J. Photochem. Photobiol. A 162 (2004) 317–322.
[3] C.A.K. Gouvea, F. Wypych, S.G. Moraes, N. Duran, N. Nagata, P. Peralta-Zamora, Chemosphere 40 (2000) 433–440.
[4] B. Dindar, S. Icli, J. Photochem. Photobiol. A: Chem. 140 (2001) 263–268.
[5] C. Gu, C. Cheng, H. Huang, T. Wong, N. Wang, T.Y. Zhang, Cryst. Growth Des. 9 (2009) 3278–3285.
[6] X. Liu, J. Zhang, L. Wang, T. Yang, X. Guo, S. Wu, S. Wang, J. Mater. Chem. 21 (2011) 349–356.
[7] X.-Y. Xue, Z.-H. Chen, L.-L. Xing, C.-H. Ma, Y.-J. Chen, T.-H. Wang, J. Phys. Chem. C 114 (2010) 18607–18611.
[8] Y. Zheng, L. Zheng, Y. Zhan, X. Lin, Q. Zheng, K. Wei, Inorg. Chem. 46 (2007) 6980–6986.
[9] F. Lu, W. Cai, Y. Zhang, Adv. Funct. Mater. 18 (2008) 1047–1056.
[10] A. Dawson, P.V. Kamat, J. Phys. Chem. B 105 (2001) 960–965.
[11] H. Tada, K. Teranishi, Y. Inubushi, S. Ito, Langmuir 16 (2000) 3304–3309.
[12] W. Lu, S. Gao, J. Wang, J. Phys. Chem. C 112 (2008) 16792–16800.
[13] A. Mills, C.E. Holland, R.H. Davies, D. Worsley, J. Photochem. Photobiol. A 83 (1994) 257–263.
[14] A. Panacek, L. Kvitek, R. Prucek, M. Kolar, R. Vecerova, N. Pizurova, V.K. Sharma, T. Nevecna, R. Zboril, J. Phys. Chem. B 110 (2006) 16248–16253.
[15] A.M. Cao, J.S. Hu, H.P. Liang, W.G. Song, L.J. Wan, X.L. He, X.G. Gao, S.H. Xia, J. Phys. Chem. B 110 (2006) 15858–15863.
[16] A. Cao, J.D. Monnell, C. Matranga, J. Wu, L. Cao, D. Gao, J. Phys. Chem. C 111 (2007) 18624–186428.
[17] S. Gao, H. Zhang, X. Wang, R. Deng, D. Sun, G. Zheng, J. Phys. Chem. B 110 (2006) 15847–15852.
[18] J.G. Yu, J.F. Xiong, B. Cheng, S.W. Liu, Appl. Catal. B 60 (2005) 211–221.
[19] L.Q. Jing, Z.L. Xu, J. Shang, W.M. Cai, H.C. Guo, Mater. Sci. Eng. A 332 (2002) 356–361.
[20] Y. Du, M.-S. Zhang, J. Hong, Y. Shen, Q. Chen, Z. Yin, Appl. Phys. A 76 (2003) 171–176.
[21] N.S. Ramgir, I.S. Mulla, V.K. Pillai, J. Phys. Chem. B 110 (2006) 3995–4001.
[22] A.L. Linsebigler, G.Q. Lu, J.T. Yates, Chem. Rev. 95 (1995) 735–758.
[23] X.Z. Li, F.B. Li, Environ. Sci. Technol. 35 (2001) 2381–2387.
[24] A. Sclafani, J.M. Herrmann, J. Photochem. Photobiol. A Chem. 113 (1998) 181–188.
[25] H. Tahiri, Y.A. Ichou, J.M. Herrmann, J. Photochem. Photobiol. A Chem. 114 (1998) 219–226.
[26] I.M. Arabatzis, T. Stergiopoulos, D. Andreeva, S. Kitova, S.G. Neophytides, P. Falaras, J. Catal. 220 (2003) 127–135.
[27] A. Sclafani, L. Palmisano, M. Schiavello, J. Phys. Chem. 94 (1990) 829–832.
[28] K. Chhor, J.F. Bocquet, C. Colbeau-Justin, Mater. Chem. Phys. 86 (2004) 123–131.
[29] X. Wang, C.J. Summers, Z.L. Wang, Appl. Phys. Lett. 86 (2005) 013111-1–013111-3.
[30] D.A. Neamen, Semiconductor Physics and Devices: Basic Principles, third ed., McGraw-Hill Professional, New York, 2003.